JPEDAV (2006) 27:22-29
DOI: 10.1361/105497106X92763
1547-7037/$19.00 ©ASM International

Modeling of Microstructure Changes in Fe-Cr-Co Magnetic Alloy Using the Phase-Field Method

Toshiyuki Koyama and Hidehiro Onodera

(Submitted December 28, 2004; in revised form February 25, 2005)

During the last decade, the phase-field method has emerged in many fields if materials science as a powerful tool to simulate and predict complex microstructure development. In this study, the microstructure changes during thermomagnetic treatment and step aging of the Fe-Cr-Co magnetic alloy are modeled using phase-field methods. Using phase-field simulation, the model reasonably represented microstructural changes in the Fe-Cr-Co system quantitatively. In particular, it is shown that gradual step aging is important to obtain the lamellar microstructure that provides excellent permanent magnetic properties. Modeling of microstructure development with the framework of the phase-field method is shown to be a very effective strategy to predict and analyze complex microstructure formation.

Keywords computer simulation, diffusion equation, magnetic aging, phase decomposition, phase transformation, spinodal decomposition, step aging

1. Introduction

Because the factors effecting on the formation of microstructure are manifold, e.g., alloy composition, heat treatment condition, etc., much experimental trial-and-error is necessary in the search for the optimum microstructure with the best material properties, even if a basic mechanism of the microstructural formation is understood. During the last decade, however, the phase-field method[1-7] has been developed in many fields of materials science as a powerful tool to simulate and predict complex microstructure development (dendrite growth, spinodal decomposition, Ostwald ripening, crystal growth, recrystallization, martensitic transformation, dislocation dynamics, electromigration, crack propagation, etc.). Because the phase-field method can model various complex microstructure changes quantitatively, it will be possible to search for the most desirable microstructure by using this method for design simulation, i.e., computer-based trial-and-error testing. Therefore, the most efficient strategy for developing advanced materials would be as follows: first, elucidate the mechanism of microstructure changes experimentally; then model the microstructure development with the framework of the phase-field method using the experimental results; and finally, search for the most desirable microstructure while simultaneously considering both the simulation and the experiment.

This paper was presented at the International Symposium on User Aspects of Phase Diagrams, Materials Solutions and Exposition, Columbus, Ohio, 18-20 October, 2004.

Toshiyuki Koyama and **Hidehiro Onodera,** Computational Materials Science Center, National Institute for Materials Science, 1-2-1 Sengen, Tsukuba, Ibaraki 305-0047, Japan. Contact e-mail: Koyama.Toshiyuki@nims.go.jp.

To carry out this methodology, a quantitative flexible modeling method for the complex microstructural changes must be established for use of phase-field simulation. In this work, "modeling the microstructure changes within the framework of the phase-field method" is called "phase-field modeling"[8,9] for simplicity. Phase-field modeling from a practical viewpoint is aimed at decreasing the frequency of experimental trial-and-error testing as much as possible through the computer simulations.

The objective of this study is to model the microstructural changes during thermomagnetic treatment and step aging of the Fe-Cr-Co magnetic alloy, which serves as a typical example of this approach. The sequence for obtaining an excellent permanent magnet of Fe-Cr-Co alloy has been explained as follows[10]: Fig. 1(a) shows a schematic illustration of an isothermal section of the Fe-Cr-Co diagram, and Fig. 1(b) shows a vertical section along the dash-dot line A-B in Fig. 1(a). The α_1 phase is ferromagnetic existing in the concentration region Fe contiguous to the CoFe boundary; on the other hand, the α_2 phase is a Cr-rich paramagnetic existing at Cr-rich compositions. The magnetic transition is represented by the dash-dot line, and the magnetic transition line extends into the ($\alpha_1 + \alpha_2$) two-phase region, as shown at the top part of the miscibility gap in Fig. 1(b). To obtain a microstructure suitable for an excellent permanent magnet, a specimen of the average composition, c_0, is annealed at T_1; this produces a supersaturated solid solution of α phase. The alloy is then treated thermomagnetically, i.e., the specimen is aged under an external magnetic field at the temperature T_2, which is just below the Curie temperature. A schematic illustration of the microstructure resulting from the thermomagnetic treatment is shown (Fig. 1c), where the white particles are the ferromagnetic α_1 phase and the black matrix is the paramagnetic α_2 phase. The morphology of α_1 precipitate is rod shaped and elongated along the external magnetic field indicated by the thick arrow in Fig. 1(c). After thermomagnetic treatment at T_2, the specimen is step aged from T_2 to T_3, and the morphology of microstructure changes from Fig. 1(c) to Fig. 1(d) during the step aging. At the temperature T_2, because

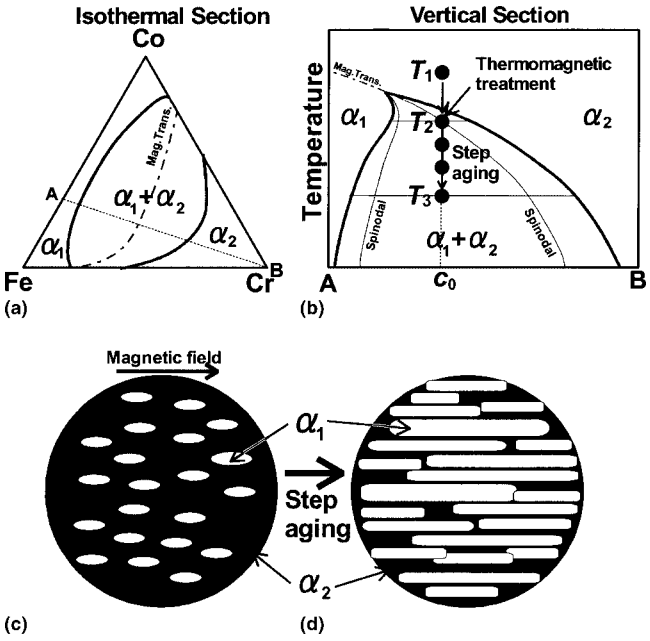

Fig. 1 Schematic illustrations of the phase diagram and the microstructure changes of Fe-Cr-Co alloy system, which explain the sequence to obtain an excellent microstructure for a permanent magnet

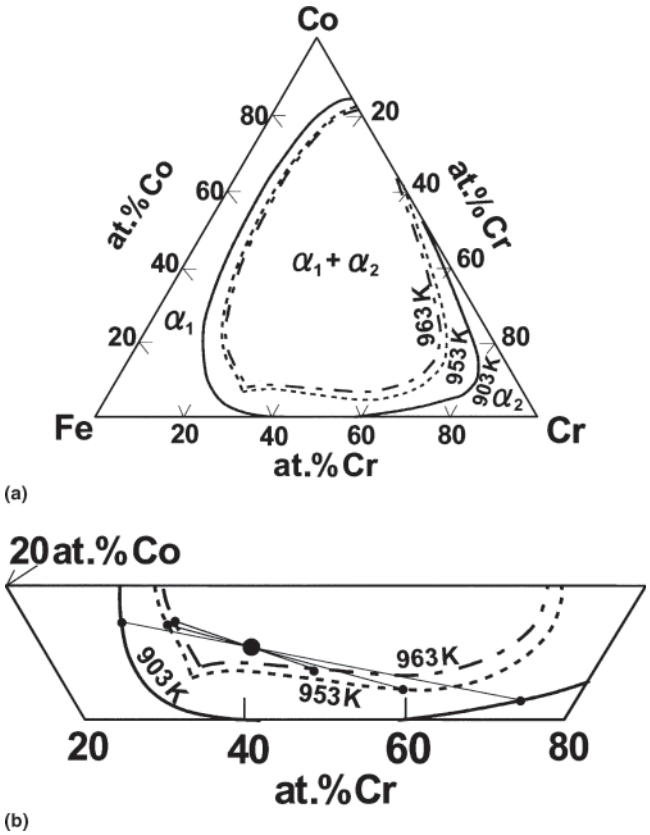

Fig. 2 Calculated metastable phase diagram of Fe-Cr-Co system

the volume fraction of α_1 phase is smaller than that of α_2 phase, the initial nucleation phase should be α_1, as illustrated in Fig. 1(c). During step aging, α_1 particles grow extensively, as represented in Fig. 1(d), because the volume fraction of α_1 phase is larger than that of α_2 phase at low temperature, T_3. It is well known that the lamellar shaped morphology of the microstructure of Fig. 1(d) has a large volume fraction of ferromagnetic rod-shaped α_1 phase that is surrounded by a thin layer of paramagnetic α_2 phase. This microstructure is suitable as an excellent permanent magnet.[11,12] In this study, this complex microstructure sequence is modeled using phase-field modeling.

2. Simulation Method

2.1 Total Free Energy of Microstructure

To simulate the microstructure changes quantitatively, the precise evaluation of total free energy functional of the microstructure is required. The total free energy of the inhomogeneous system is expressed as[13]:

$$G_{sys} = \int_{\mathbf{r}} \left[G_c^{\alpha}\{c_i(\mathbf{r},t),T\} + \frac{1}{2}\kappa_c \sum_{i=1}^{3} \{\nabla c_i(\mathbf{r},t)\}^2 \right] d\mathbf{r} + E_{str}(t) + E_{mag}(t,T) \quad \text{(Eq 1)}$$

where G_c^{α} is the Gibbs energy density and T is temperature. E_{str} and E_{mag} are the elastic strain energy and the magnetic energy, respectively. The second term in the square bracket is the composition gradient energy,[14] where κ_c is the composition gradient energy coefficient and is assumed to be constant in this study. $c_i(\mathbf{r},t)$ is the local composition of the component i at position $\mathbf{r}$ and time t in the microstructure. The subscript numbers $i = 1$, 2, and 3 refer to Fe, Cr, and Co, respectively.

The Gibbs free energy of the α(bcc) phase of the Fe-Cr-Co system with magnetic contribution is described by the subregular solution approximation[15]:

$$G_c^{\alpha}(c_i,T) = \sum_{i=1}^{3} {}^{\circ}G_i^{\alpha} c_i + RT \sum_{i=1}^{3} c_i \ln c_i + {}^{E}G^{\alpha} + {}^{mg}G^{\alpha} \quad \text{(Eq 2)}$$

$${}^{E}G^{\alpha} \equiv L_{1,2}^{\alpha} c_1 c_2 + L_{1,3}^{\alpha} c_1 c_3 + L_{2,3}^{\alpha} c_2 c_3 \quad \text{(Eq 3)}$$

$${}^{mg}G^{\alpha} \equiv RT \ln(\beta^{\alpha} + 1) f(\tau) \quad \text{(Eq 4)}$$

where ${}^{\circ}G_i^{\alpha}$ is the standard Gibbs energy of pure component i in the case of bcc crystal structure. R is the gas constant. ${}^{E}G^{\alpha}$ is the excess free energy corresponding to the heat of mixing, and ${}^{mg}G^{\alpha}$ is the magnetic contribution to the Gibbs energy. The parameter τ is a dimensionless temperature normalized by Curie temperature T_C^{α}, i.e., defined by $\tau \equiv T/T_C^{\alpha}$. The interaction parameter $L_{i,j}^{\alpha}$, the Curie temperature T_C^{α}, and the atomic magnetic moment β^{α} are available from the thermodynamic databases of equilibrium phase diagrams, such as the SGTE database,[15] and the following data were also used[16]:

$$L^{\alpha}_{1,2} = 20{,}500 - 9.68T$$

$$L^{\alpha}_{1,3} = -23{,}669 + 103.9627T - 12.7886T\ln T$$

$$L^{\alpha}_{2,3} = (24{,}357 - 19.797T) - 2010(c_3 - c_2) \text{ (in J mol}^{-1}\text{)}$$

$$T^{\alpha}_{C} = 1043c_1 - 311.5c_2 + 1450c_3 + \{1650 + 550(c_2 - c_1)\}c_1c_2 + 590c_1c_3 \text{ (in K)}$$

and

$$\beta^{\alpha} = 2.22c_1 - 0.01c_2 + 1.35c_3 - 0.85c_1c_2 + \{2.4127 + 0.2418(c_3 - c_1)\}c_1c_3 \text{ (Bohr magneton unit)} \quad \text{(Eq 5)}$$

where $f(\tau)$ in Eq 4 is obtained as a function[15] of τ.

The crystal structure considered in this simulation is bcc only, so that ${}^{\circ}G^{\alpha}_1 = {}^{\circ}G^{\alpha}_2 = {}^{\circ}G^{\alpha}_3 = 0$ was adopted as the reference energy level for the Gibbs free energy.

The elastic strain energy,[17,18] E_{str}, is represented as:

$$E_{str}(t) = \frac{1}{2}\int_{\mathbf{r}} C_{ijkl}\varepsilon^{el}_{ij}(\mathbf{r},t)\varepsilon^{el}_{kl}(\mathbf{r},t)d\mathbf{r}$$

$$\varepsilon^{el}_{ij}(\mathbf{r},t) \equiv \varepsilon^{c}_{ij}(\mathbf{r},t) - \varepsilon^{0}_{ij}(\mathbf{r},t) \quad \text{(Eq 6)}$$

where $\varepsilon^{el}_{ij}(\mathbf{r},t)$ is elastic strain and C_{ijkl} is the elastic constant. The stress-free strain,[17,18] $\varepsilon^{0}_{ij}(\mathbf{r},t)$, is given by:

$$\varepsilon^{0}_{ij}(\mathbf{r},t) = [\varepsilon_2\{c_2(\mathbf{r},t) - c^0_2\} + \varepsilon_3\{c_3(\mathbf{r},t) - c^0_3\}]\delta_{ij} \quad \text{(Eq 7)}$$

where ε_i is the lattice mismatch, c^0_i is the average composition of component i, and δ_{ij} is the Kronecker delta. The constrained strain, $\varepsilon^{c}_{ij}(\mathbf{r},t)$, is obtained from:

$$\varepsilon^{c}_{kl}(\mathbf{r},t) = \int_{\mathbf{k}}\left[\Omega_{ik}(\mathbf{n})n_jn_lC_{ijpq}\delta_{pq}\begin{Bmatrix}\varepsilon_2\hat{c}_2(\mathbf{k},t)\\ +\varepsilon_3\hat{c}_3(\mathbf{k},t)\end{Bmatrix}\right]\exp(i\mathbf{k}\cdot\mathbf{r})\frac{d\mathbf{k}}{(2\pi)^3} \quad \text{(Eq 8)}$$

where $\Omega_{ik}(\mathbf{n})$ is the inverse matrix of $\Omega^{-1}_{ik}(\mathbf{n}) \equiv C_{ijkl}n_jn_l$. $\mathbf{k}$ is a reciprocal space vector and $\mathbf{n} \equiv \mathbf{k}/|\mathbf{k}|$ is a unit vector along the $\mathbf{k}$ direction. $\hat{c}_i(\mathbf{k},t)$ is the Fourier transform of the $c_i(\mathbf{r},t)$ field.

The magnetic energy E_{mag} depends on the inhomogeneous morphology of the magnetic domain microstructure. Therefore, $E_{mag} = 0$ when the magnetic moment $\mathbf{M}(\mathbf{r},t)$ takes a uniform equilibrium value throughout the material and the direction of the vector is along the axis of easy magnetization. Therefore, the magnetic energy for a single ferromagnetic phase with infinite size is included in ${}^{mg}G^{\alpha}$ in Eq 2.

As for the evaluation of magnetic energy E_{mag}, only the demagnetizing energy $E_d(t)$ was considered because it is already understood that the phase decomposition targeted in this study is influenced mainly by $E_d(t)$.[11,12] The physical meaning of $E_d(t)$ is the dipole-dipole interaction energy between magnetic moments, and that is expressed as[17]:

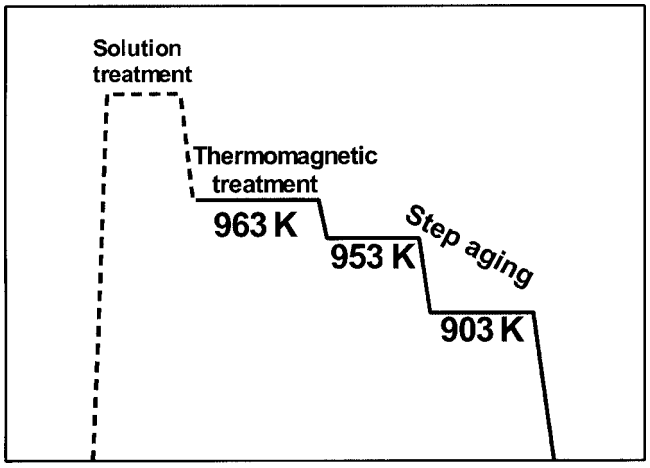

Fig. 3 Schematic illustration of heat treatment used for the simulation

$$E_d(t) = \frac{1}{2\mu_0}\sum_{i=2}^{3}\sum_{j=2}^{3}\int_{\mathbf{r}}\int_{\mathbf{r}'}\left[\begin{array}{l}\left(\frac{\partial M_S}{\partial c_i}\right)_{c^0_2,c^0_3}\{c_i(\mathbf{r},t) - c^0_i\}m_k(\mathbf{r})\\ \times W_{kl}(\mathbf{r}-\mathbf{r}')m_l(\mathbf{r}')\left(\frac{\partial M_S}{\partial c_j}\right)_{c^0_2,c^0_3}\{c_j(\mathbf{r}',t) - c^0_j\}\end{array}\right]d\mathbf{r}d\mathbf{r}' \quad \text{(Eq 9)}$$

$$W_{ij}(\mathbf{r}-\mathbf{r}') \equiv \frac{1}{4\pi}\left(\frac{\delta_{ij}}{|\mathbf{r}-\mathbf{r}'|^3} - \frac{3(r_i - r'_i)(r_j - r'_j)}{|\mathbf{r}-\mathbf{r}'|^5}\right) \quad \text{(Eq 10)}$$

where μ_0 is the permeability of vacuum. M_S is the absolute value of magnetization moment vector, which depends on the local composition and temperature. The vector $\mathbf{m}(\mathbf{r})$ is the normalized magnetization moment ($|\mathbf{m}(\mathbf{r})| = 1$).

It is known that the intensity of magnetization, $I(\tau)$, which is normalized by saturation magnetization, is expressed theoretically by the Brillouin function.[19] In this calculation, the function for the analytical form is estimated as follows[13]:

$$I(\tau) = 1 - \frac{1}{7}(5\tau^4 + 2\tau^{20}) \quad (\tau \le 0.9)$$

$$I(\tau) = 2^{-\{2+10(\tau-1)\}} \quad (\tau > 0.9) \quad \text{(Eq 11)}$$

where τ defines the ratio T/T^{α}_C.

With functions $I(\tau)$, $T^{\alpha}_C(c_i)$, and $\beta^{\alpha}(c_i)$, the magnetization moment vector $\mathbf{M}(\mathbf{r},t)$ is obtained as:

$$\mathbf{M}(\mathbf{r},t) = M_S(c_i,\tau)\mathbf{m}(\mathbf{r})$$

$$M_S(c_i,\tau) = \beta^0_{Bohr}\beta^{\alpha}(c_i)I(\tau) = \beta^0_{Bohr}\beta^{\alpha}(c_i)I[T/T^{\alpha}_C(c_i)] \quad \text{(Eq 12)}$$

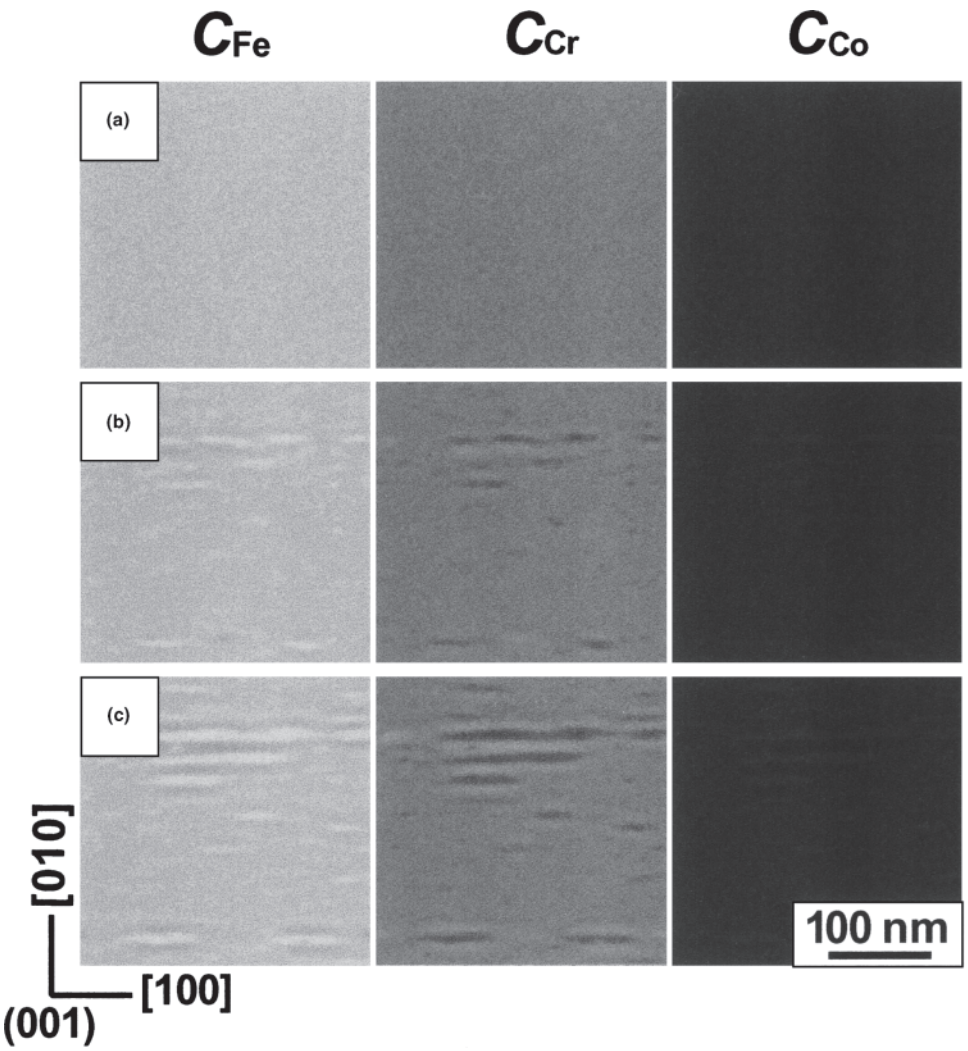

Fig. 4 Calculation of phase decomposition in Fe-35 at.% Cr-12 at.% Co alloy at 963 K under external magnetic field (thermomagnetic treatment): (a) $t' = 0$; (b) $t' = 20$; and (c) $t' = 40$

where β^0_{Bohr} is the Bohr magneton (with a unit of T). It is worth noting that $\mathbf{M}(\mathbf{r},t)$ is represented as a function of composition and temperature because $\beta^{\alpha}(c_i)$ and $\tau \equiv T/T^{\alpha}_{C}(c_i)$ depend on composition and temperature. Therefore, $\partial M_S/\partial c_i$ in Eq 9 can be calculated analytically with Eq 12.

2.2 Phase-Field Method (Governing Equations Describing Phase Decomposition and Microstructure Change)

The phase-field method is the computer simulation method for calculating the dynamics of temporal microstructure changes by solving the continuum nonlinear evolution equations for the conserved and nonconserved order parameters. In this work, because the composition field was considered only as an order parameter, the phase-field method used in this study is similar to computer simulation with the Cahn-Hilliard nonlinear diffusion equation.[14] Therefore, the evolution equations governing the phase decomposition in an Fe-Cr-Co ternary system are expressed as

$$\frac{\partial c_2}{\partial t} = \nabla \cdot \left(L_{22} \nabla \frac{\delta G_{\text{sys}}}{\delta c_2} + L_{23} \nabla \frac{\delta G_{\text{sys}}}{\delta c_3} \right)$$

$$\frac{\partial c_3}{\partial t} = \nabla \cdot \left(L_{32} \nabla \frac{\delta G_{\text{sys}}}{\delta c_2} + L_{33} \nabla \frac{\delta G_{\text{sys}}}{\delta c_3} \right) \qquad \text{(Eq 13)}$$

where the Onsager coefficients L_{ij} are determined by using the self-diffusion coefficient D_i^* as:

$$L_{22} = [c_1 c_2 D_1^* + (1 - c_2)^2 D_2^* + c_2 c_3 D_3^*] \frac{c_2}{RT}$$

$$L_{33} = [c_1 c_3 D_1^* + c_2 c_3 D_2^* + (1 - c_3)^2 D_3^*] \frac{c_3}{RT}$$

$$L_{23} = L_{32} = [c_1 D_1^* - (1 - c_2) D_2^* - (1 - c_3) D_3^*] \frac{c_2 c_3}{RT} \qquad \text{(Eq 14)}$$

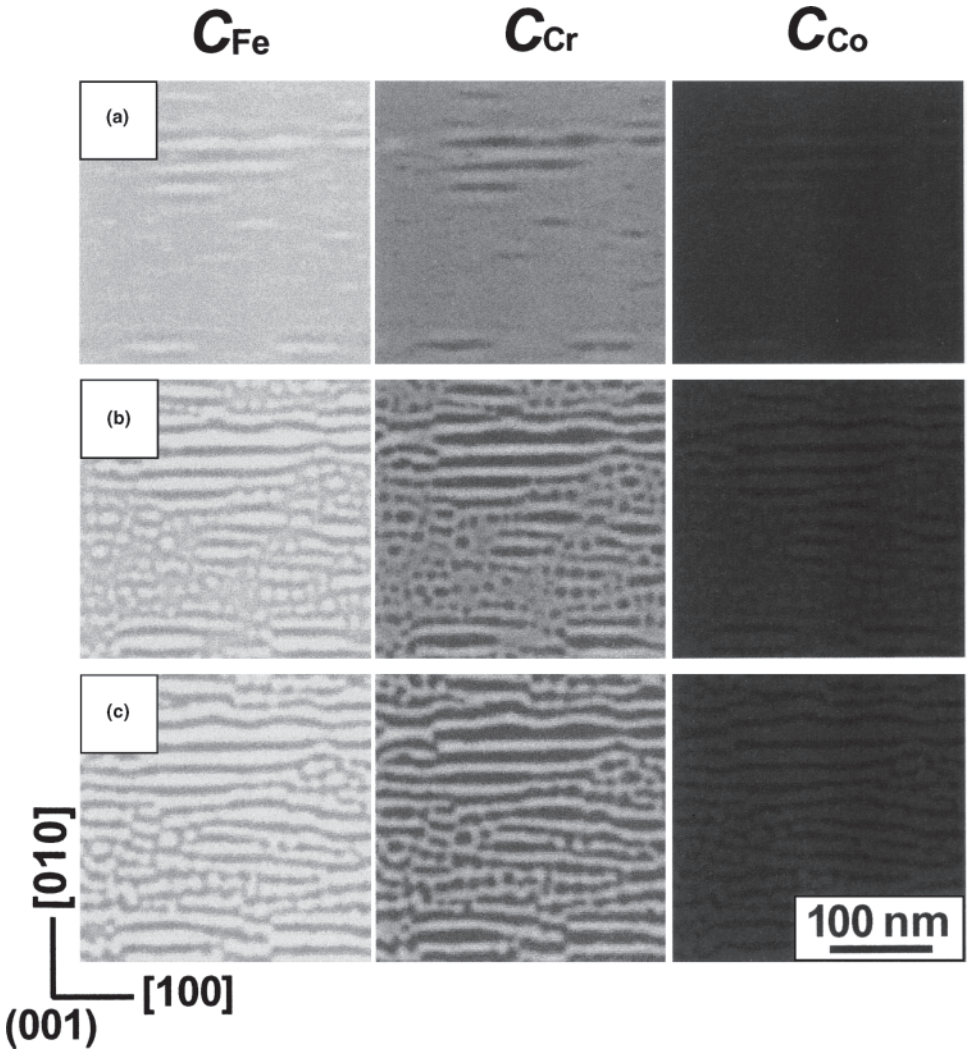

Fig. 5 Calculation of phase decomposition during the first aging step at 953 K: (a) $t' = 40$; (b) $t' = 69$; and (c) $t' = 99$

Equation 14 corresponds to a modification of the Darken relation[20] for application to a ternary system. Numerical values[21] used in the simulation are summarized in Table 1.

2.3 Calculation Conditions

Figure 2(a) shows the metastable isothermal section diagrams of the bcc phase in the Fe-Cr-Co ternary alloy at 963, 953, and 903 K, respectively, calculated using the thermodynamic parameters of Eq 5. The Fe-Cr side of Fig. 2(a) is magnified in Fig. 2(b). Note that the ($\alpha_1 + \alpha_2$) two-phase region of Fe-Cr binary phase diagram (see the case of 903 K) is wide and initially broadens with increasing Co content; although the ($\alpha_1 + \alpha_2$) two-phase region disappears at higher temperature in the Fe-Cr binary system, the two-phase region still exists in the ternary-phase diagram. The alloy composition used in the simulation is Fe-35 at.% Cr-12 at.% Co, denoted by the large solid circle in Fig. 2(b). The thin straight lines inside the two-phase region of Fig. 2(b) are the calculated tie lines.

Table 1 Numerical values used in the calculation

Temperature, T (K)	963, 953, 903
Composition gradient energy coefficient, κ_s ($J \cdot m^2 \cdot mol^{-1}$)	1.0×10^{-14}
Lattice mismatch,[21] ε_i	$\varepsilon_2 = 6.1 \times 10^{-3}$
	$\varepsilon_3 = -7.1 \times 10^{-3}$
Elastic coefficients[21] of element X (C_{ij}^X, GPa)	$C_{11}^{Fe} = 233.1$
(elastic coefficients for bcc Co are assumed to be $C_{ij}^{Co} = C_{ij}^{Fe}$.)	$C_{12}^{Fe} = 135.44$
	$C_{44}^{Fe} = 117.83$
	$C_{11}^{Cr} = 350$
	$C_{12}^{Cr} = 67.8$
	$C_{44}^{Cr} = 100.8$
Self-diffusion coefficient[21] of component i,	$D_1^0 = 1.0 \times 10^{-4}$
$D_i^* = D_i^0 \exp(-Q_i/RT)$, D_i^0 ($m^2 \cdot s^{-1}$), Q_i ($kJ \cdot mol^{-1}$)	$Q_1 = 294$
(self-diffusion coefficient for bcc Co is assumed to be $D_3^* = D_1^*$.)	$D_2^0 = 2.0 \times 10^{-5}$
	$Q_2 = 308$
Calculation area, $L \times L$ (nm^2)	350×350
Total mesh number for difference method, $N \times N$	128×128

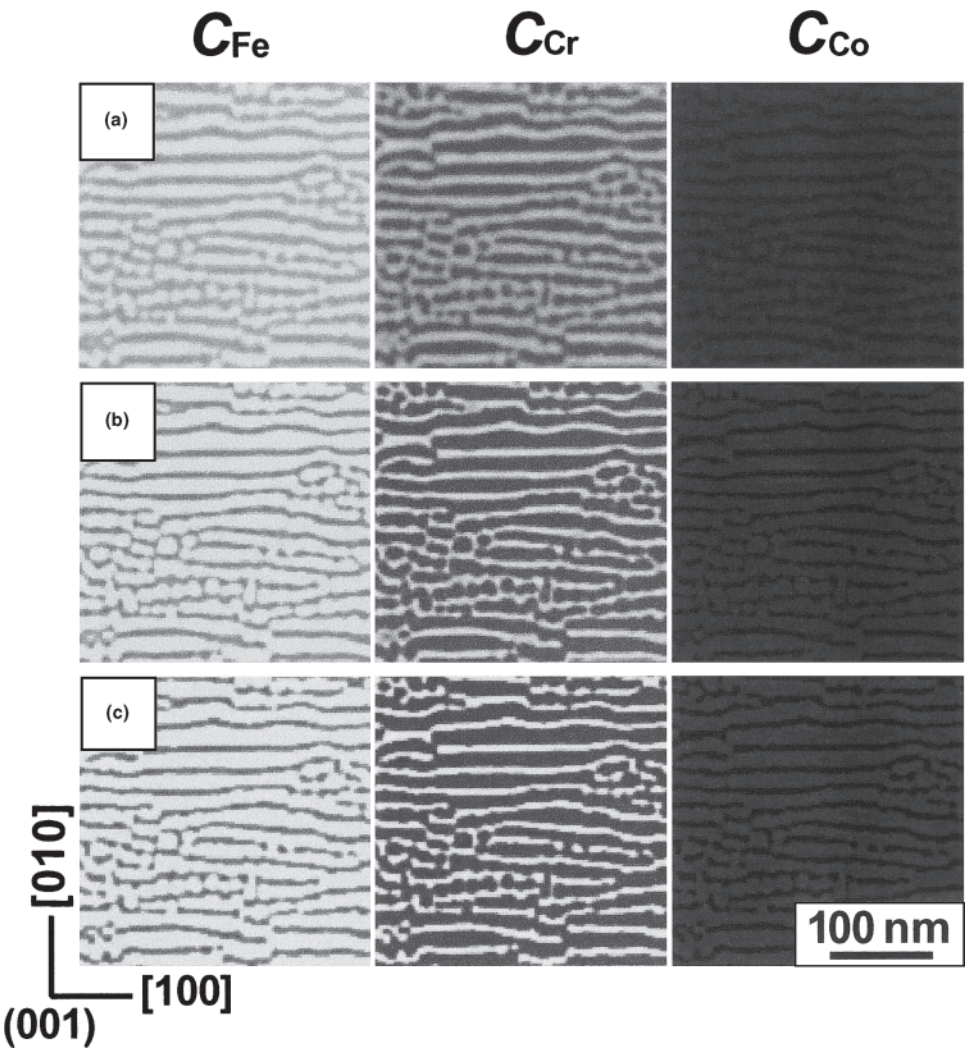

Fig. 6 Calculation of phase decomposition during the second aging step at 903 K: (a) $t' = 99$; (b) $t' = 214$; and (c) $t' = 558$

Figure 3 schematically illustrates the core treatment conditions used in the simulation. Because the initial state is assumed to be a supersaturated solid solution in the simulation, the solution treatment in Fig. 3 is attained from the initial conditions of the calculation. The simulation of phase decomposition starts at 963 K. Thermomagnetic treatment is performed at 963 K, i.e., the external magnetic field is considered at 963 K aging only. Step aging at 953 and 903 K is then simulated in the condition without external magnetic field. According to the phase diagram (Fig. 2b), the volume fraction of Fe-rich α_1 phase is relatively smaller than that of Cr-rich α_2 phase at 963 K. During step aging at 953 and 903 K, the volume fraction of the α_1 phase becomes larger and larger. Note that this volume fraction change in α_1 phase is enhanced by the tie-line rotation (Fig. 2b).

In the simulation, a three-dimensional system was considered in evaluating the elastic strain energy, but the microstructure morphology of the cross section perpendicular to the [100] direction was assumed congruent, i.e., the morphology of microstructure perpendicular to the paper surface is similar in shape. Therefore, the present calculation is essentially a two-dimensional simulation on the (100) plane. To solve Eq 13 numerically, a conventional difference method is used. The minimum mesh size, b, is defined by $b \equiv L/N$, where N is the dividing number in the x (or y) direction. The spatial distance and the aging time are normalized by using b and $b^2/D_1{}^*(T = 963\ \text{K})$, respectively, and the normalized aging time is referred to as t' herein.

3. Simulation Results and Discussions

3.1 Phase Decomposition with Thermomagnetic Treatment at 963 K

Figure 4 shows the two-dimensional simulation for the phase decomposition of α (bcc) phase at 963 K under an external magnetic field applied in the horizontal direction [100]. The average composition of the alloy is Fe-35 at.% Cr-12 at.% Co. The external magnetic field was assumed to

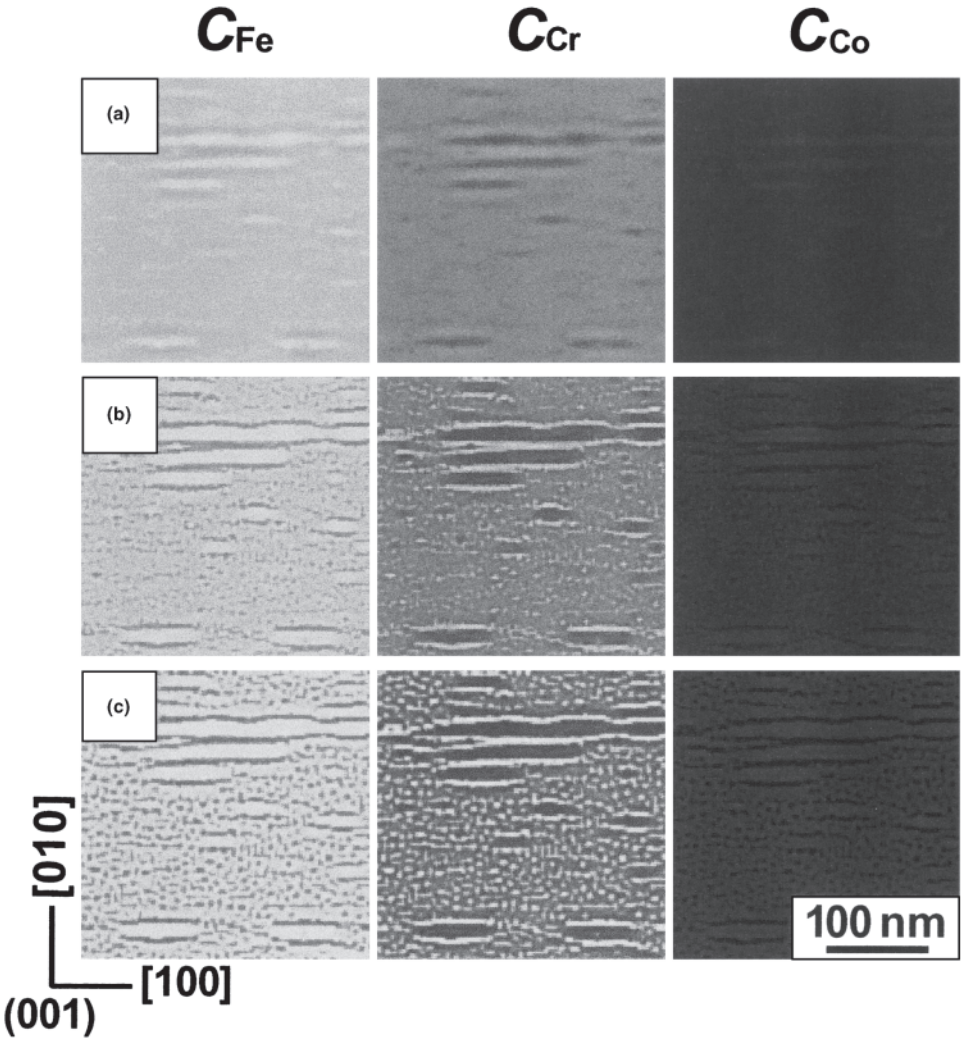

Fig. 7 Calculation of phase decomposition during the aging step at 903 K: (a) $t' = 40$; (b) $t' = 269$; and (c) $t' = 499$

be strong enough to align all magnetic spins in the direction of the external magnetic field, i.e., the normalized magnetic moment vector $\mathbf{m}(\mathbf{r},t)$ is fixed as $\mathbf{m}(\mathbf{r},t) = (1, 0, 0)$. From the top layer to the bottom layer (Fig. 4), the microstructure change during isothermal phase decomposition at 963 K is shown. Three columns of Fig. 4 correspond to the composition fields $c_1 = c_{Fe}$, $c_2 = c_{Cr}$, and $c_3 = c_{Cr}$, respectively. The local composition is represented in gray scale, and white areas represent high concentrations of the corresponding element. Figure 4(a) is the initial state of the supersaturated solid solution with small composition fluctuation that is imposed by using the random number generated in computer. With the aging progress (Fig. 4a to c), the (Fe,Co)-rich α_1 phase elongated along the external magnetic field is nucleated (Fig. 4c). Because the magnetic energy E_d increases with composition fluctuation along the direction of the magnetic moment (see Eq 9), the E_d suppresses the phase decomposition.[12] Therefore, the composition modulation along the external magnetic field does not progress. This microstructure corresponds to that represented in Fig. 1(c).

3.2 Microstructure Changes During Step Aging

In the simulation of the step aging at 953 and 903 K, the magnetic energy is not considered; the condition $E_{mag} = 0$ was assumed to simplify the simulation. The first step aging process at 953 K produces microstructure changes from Fig. 5(a) to (c), where the initial microstructure in Fig. 5(a) is the same as in Fig. 4(c). The manner for drawing the figure is the same as Fig. 4. When the microstructure changes of Fe-composition field c_{Fe} from Fig. 5(a) to (c) are examined, the Fe-rich α_1 phase (the white part in the figure) is further nucleated and the number of α_1 precipitates is increased. In the simulated microstructure shown in Fig. 5, although the external magnetic field is turned off, the global morphology of the final microstructure maintains a lamellar shape (Fig. 5c).

The microstructure changes during the second step aging process at 903 K is represented in Fig. 6, with the microstructure represented in Fig. 5(c) being used as the initial microstructure (Fig. 6a). With aging, both the Fe composition in the α_1 phase and the Cr composition in the α_2 phase

are increased, which is clearly seen in the contrast changes from Fig. 6(a) to (c). When the α_1 phase (white part of the composition field c_{Fe}) in the lamellar structure is examined more closely, the width of α_1 phase increases as aging time progresses, i.e., the volume fraction of α_1 phase increases with aging. The microstructure changes demonstrated in Fig. 5 and 6 correspond to the schematic illustration of the microstructure evolution from Fig. 1(c) to (d). The morphological and temporal developments of the simulated microstructures are in good agreement with experimental results[22,23] that have been observed in this alloy system.

Figure 7 shows the simulation result of the isothermal phase decomposition at 903 K. In this case, the first step aging process at 953 K was skipped and the simulation at 903 K is started directly after thermomagnetic treatment at 963 K; therefore the initial microstructure (Fig. 7a) is the same as Fig. 4(c). It is noted that the very fine α_2 phase particles are nucleated and thus the global lamellar microstructure cannot be obtained. From this result, it is understood that gradual multistep aging from the high temperature to the low temperature is very important for maintaining the lamellar microstructure.

4. Conclusions

The microstructure changes during thermomagnetic treatment and the step aging in Fe-Cr-Co magnetic alloy were modeled using the phase-field method. The results obtained are as follows:

- Microstructure changes during thermomagnetic treatment and step aging are simulated by phase-field method reasonably well. This simulation model suggests that process optimization will be possible through trial-and-error testing using phase-field modeling.
- Phase-field simulation linked to thermodynamic databases of phase diagrams will be quite useful to design microstructures in real alloy systems. In particular, thermodynamic databases are applicable not only for Gibbs energy estimation but also for magnetic energy evaluation.
- Gradual multistep aging from the high temperature to the low temperature is very important for maintaining the lamellar microstructure. The modeling of microstructure developments within the framework of the phase-field method will be very effective strategy to predict and analyze complex microstructure formation.

Acknowledgments

This work was partly supported by a NEDO International Joint Research Grant on "Structuring Knowledge, Science and Technology for Nano Material Processing" and "Nanometal Technology Project" and by the Special Coordination Funds for Promoting Science and Technology on "Nanoheterometallic Materials" from the Ministry of Education, Culture, Sport, Science and Technology. This work was also supported by the NAREGI Nanoscience Project; the Ministry of Education, Culture, Sports, Science and Technology; and CREST (Japan Science and Technology Agency).

References

1. R. Kobayashi, Modeling and Numerical Simulations of Dendritic Crystal Growth, *Physica D,* 1993, 63, p 410-423
2. A.A. Wheeler, W.J. Boettinger, and G.B. McFadden, Phase-Field Model for Isothermal Phase Transitions in Binary Alloys, *Phys. Rev. A,* 1992, 45A, p 7424–7439
3. W.J. Boettinger, J.A. Warren, C. Beckermann, and A. Karma, Phase-Field Simulation of Solidification, *Annu. Rev. Mater. Res.,* 2002, 32, p 163-194
4. L.-Q. Chen, Phase-Field Models for Microstructure Evolution, *Annu. Rev. Mater. Res.,* 2002, 32, p 113-140
5. M. Ode, S.G. Kim, and T. Suzuki, Recent Advances in the Phase-Field Model for Solidification, *ISIJ Int.,* 2001, 41, p 1076-1082
6. H. Emmerich, *The Diffuse Interface Approach in Materials Science,* Springer-Verlag, Berlin, 2003
7. D. Raabe, *Computational Materials Science,* Wiley-VCH, Weinheim, 1998
8. T. Koyama and H. Onodera, Modeling of Microstructure Changes in FePt Nano-Granular Thin Films Using the Phase-Field Method, *Mater. Trans. JIM,* 2003, 44, p 1523-1528
9. T. Koyama and H. Onodera, Phase-Field Simulation of Microstructure Changes in Ni_2MnGa Ferromagnetic Alloy Under External Stress and Magnetic Fields, *Mater. Trans. JIM.,* 2003, 44, p 2503-2508
10. S.M. Hao, K. Ishida, and T. Nishizawa, Role of Alloying Element in Phase Decomposition in Alnico Magnet Alloys, *Metal. Trans. A,* 1985, 16A, p 179-185
11. Y. Iwama and M. Takeuchi, Spinodal Decomposition in Alnico 8 Magnet Alloy, *Trans. JIM,* 1974, 15, p 371-377
12. J.W. Cahn, Magnetic Aging of Spinodal Alloys, *J. Appl. Phys.,* 1963, 34, p 3581-3586
13. T. Koyama and H. Onodera, Phase-Field Simulation of Phase Decomposition in Fe-Cr-Co Alloy Under External Magnetic Field, *Met. Mater. Int.,* 2004, 10, p 321-326
14. J.E. Hilliard, Spinodal Decomposition, in *Phase Transformation,* H.I. Aaronson, Ed., ASM, 1970, p 497-560
15. N. Saunders and A.P. Miodownik, *CALPHAD,* R.W. Cahn, Ed., Pergamon, Oxford, U.K., 1998
16. THERMO-CALC, Ver. M, Thermo-Calc Software AB, Stockholm
17. A.G. Khachaturyan, *Theory of Structural Transformations in Solids,* Wiley & Sons, New York, 1983
18. T. Mura, *Micromechanics of Defects in Solids,* 2nd rev. ed., Kluwer Academic, Dordrecht, The Netherlands, 1991
19. S. Chikazumi, *Physics of Ferromagnetism,* 2nd ed., Oxford University Press, New York, 1997
20. M.E. Glicksman, *Diffusion in Solids,* Wiley & Sons, New York, 2000
21. *Metals Data Book,* Japan Institute of Metals, Maruzen, Tokyo, Japan, 1993
22. M. Okada, G. Thomas, M. Homma, and H. Kaneko, Microstructure and Magnetic Properties of Fe-Cr-Co Alloys, *IEEE Trans. Magn.,* 1978, 14, p 245-252
23. T. Minowa, M. Okada, and M. Homma, Further Studies of the Miscibility Gap in an Fe-Cr-Co Permanent Magnet System, *IEEE Trans. Magn.,* 1980, 16, p 529-533